Letter | Editors' Suggestion | Featured in Physics

Nuclear magnetic resonance far off the Larmor frequency: Nonsecular resonances in CaF_2

Michael Jurkutat,[1,*] Kajum Safiullin,[1] Pooja Singh,[1] Stephan L. Grage,[2] Jürgen Haase,[3] Boris V. Fine,[4] and Benno Meier[1,5,†]

[1]*IBG-4 Magnetic Resonance, Karlsruhe Institute of Technology, Hermann-von-Helmholtz-Platz 1, 76344 Eggenstein-Leopoldshafen, Germany*

[2]*IBG-2 Molecular Biophysics, Karlsruhe Institute of Technology, Hermann-von-Helmholtz-Platz 1, 76344 Eggenstein-Leopoldshafen, Germany*

[3]*Felix-Bloch Institute for Solid State Physics, University of Leipzig, Linnéstraße 5, 04103 Leipzig, Germany*

[4]*Institute for Theoretical Physics, University of Leipzig, Brüderstraße 16, 04103 Leipzig, Germany*

[5]*Institute of Physical Chemistry, Karlsruhe Institute of Technology, Fritz-Haber-Weg 2, 76131 Karlsruhe, Germany*

(Received 12 March 2025; revised 26 June 2025; accepted 27 June 2025; published 11 August 2025)

High field magnetic resonance of nuclear spins is normally carried out at or near the Larmor frequency Ω_0. Here, we report an observation of nonsecular nuclear spin resonances far off Ω_0. These originate from nonsecular terms of the nuclear spin-spin interaction and provide means for the control of coupled two level systems. In systems of equivalent nuclear spins, nonsecular resonances were predicted to lead to anomalous, fast relaxation of the nuclear spin polarization. We report experimental results that are in excellent agreement with the predicted behavior.

DOI: 10.1103/h2sn-wvzm

Introduction. Magnetic resonance is an indispensable tool for investigating the microscopic properties of matter. The power of magnetic resonance derives from the ability to selectively excite specific resonances and thereby measure individual spin interactions from which in turn structure and dynamics can be inferred.

The primary notion of resonance originates from matching the frequency of an applied oscillating magnetic field $B_1(t)$ to the Larmor precession of a spin in a stronger static magnetic field B_0. On resonance, the resulting spin motion, the Rabi rotation, is exploited by electron spin resonance (ESR), nuclear magnetic resonance (NMR), and by quantum optics where any two-level quantum system can be treated as an effective quantum spin 1/2.

Beyond the primary spin resonance, one can control spin dynamics by exploiting other kinds of resonances. An important example is the Hartmann-Hahn matching of Rabi rotation frequencies of two different nuclear spin species that facilitates cross polarization [1]. In the NOVEL experiment [2], on the other hand, one matches the electron Rabi frequency to the nuclear Larmor frequency to facilitate electron-nuclear polarization transfer. Other reported resonances may give rise to observable coherences. In single spin systems these include multiquantum resonances in quadrupolar spins [3,4] and multiphoton transitions that involve simultaneous irradiation at two distinct frequencies [5]. In strongly coupled spin pairs it is possible to drive a $\Delta M = 2$ transition known as the half-field transition [6].

A different many-body effect, known as "nonsecular resonance" (NSR), has been predicted theoretically [7,8], but not verified experimentally to date. NSRs change effective spin-spin interaction in solids once certain resonant conditions on a strong static magnetic field B_0 and on the amplitude and the frequency of a *strong* radio-frequency (rf) field $B_1(t)$ are satisfied. The emerging unusual spin-spin interaction terms have, so far, been discarded in magnetic resonance, yet they offer a tool for controlling spin dynamics in solids. In contrast to a typical setting for multiquantum or multiphoton transitions, where the frequency of a *weak* field $B_1(t)$ targets differences of well-defined energy levels of isolated spins or spin pairs, NSRs are well defined not only for dilute but also for dense spin systems, where individual energy levels cannot be defined. In the latter case, they can cause an anomalous spin-spin relaxation.

The canonical view of effective spin-spin interactions in NMR was developed in seminal papers by Van Vleck [9] and Redfield [10]. Van Vleck showed that the full nuclear spin-spin interaction in the presence of a much stronger Zeeman coupling to a static external magnetic field must be truncated to retain only those interaction terms that commute with the Zeeman Hamiltonian. The truncation procedure is equivalent to a time average of all interaction terms in the Larmor rotating frame. Terms that do not commute with the Zeeman interaction average to zero. Redfield considered the simultaneous effects of a static B_0 and oscillating rf B_1 field and applied a second truncation by averaging the Van Vleck interaction Hamiltonian over the motion of an otherwise isolated spin under the combined action of B_0 and B_1.

The secular Van Vleck–Redfield truncation, based on the above two steps, has since then become a standard notion of NMR [11–14] and is considered valid as long as $B_0 \gg B_1$.

*Contact author: michael.jurkutat@kit.edu

†Contact author: benno.meier@kit.edu

In general, however, a rigorous procedure for evaluating the effective Hamiltonian must average the full spin-spin interaction simultaneously over the combined action of both fields B_0 and $B_1(t)$ in one step. As was shown much later by Kropf and Fine [7] this procedure leads to resonant exceptions from the secular truncation. These NSRs occur at a set of sufficiently commensurate ratios of the relevant rotation frequencies. [A somewhat similar effect due to frequency matching occurs in resonant tori in the context of the Kolmogorov-Arnold-Moser (KAM) theory of nearly integrable motion [15–19].]

The rigorously averaged dipolar Hamiltonian for equivalent nuclear spins exhibits a total of five NSRs that appear at *commensurate fractions* of the Larmor frequency Ω_0 [20]. with the lowest resonance at $1/3\,\Omega_0$ [21] and the highest at $2\Omega_0$ [7]. Note that NSRs are a general property of dipolar coupled spin systems.

Unlike the secular terms of the spin-spin interaction, the nonsecular ones do not conserve any projection of the net magnetization and it has been, therefore, predicted that they drive anomalous, dissipative longitudinal relaxation.

It is this prediction [8] that we experimentally confirm in the present work on the basis of fast-field-cycling ^{19}F NMR experiments in CaF_2. In CaF_2, the fluorine spins form an otherwise isolated simple cubic lattice of spins 1/2, making it ideally suited to study the dipolar interaction [9,22–24].

Secular truncation and nonsecular resonances. Let us consider a lattice of identical quantum spins 1/2 represented by operators $\boldsymbol{I}_i$, where i is the lattice site index. The spins are coupled to each other via magnetic dipolar coupling described by the Hamiltonian

$$\mathcal{H}_{\mathrm{DD}} = \sum_{i<j}^{N} b_{ij}\left[\boldsymbol{I}_i\boldsymbol{I}_j - \frac{3(\boldsymbol{I}_i\cdot\boldsymbol{r}_{ij})(\boldsymbol{I}_j\cdot\boldsymbol{r}_{ij})}{r_{ij}^2}\right], \tag{1}$$

where $b_{ij} = \frac{\gamma^2\hbar^2}{r_{ij}^3}$, $\boldsymbol{r}_{ij}$ is the displacement vector between sites i and j, γ is the gyromagnetic ratio, and $\hbar$ is the Planck constant. The lattice is placed in a static field $\boldsymbol{B}_0 = (0, 0, B_0)$ and a perpendicular time-dependent rf field is applied $\boldsymbol{B}_1(t) = (B_1\cos\omega t, B_1\sin\omega t, 0)$, where ω is the rf frequency. We also denote the Larmor frequency $\Omega_0 = \gamma B_0$ (in keeping with the sign convention of Ref. [7], see also Table I), the nutation frequency $\Omega_1 = \gamma B_1$, and consider the limit $\hbar\Omega_0, \hbar\Omega_1 \gg |b_{ij}|$. The corresponding Hamiltonians are $\mathcal{H}_{\mathrm{Z}} = -B_0\cdot\sum_i^N \gamma\boldsymbol{I}_i^z$ and $\mathcal{H}_{\mathrm{rf}} = -\boldsymbol{B}_1(t)\cdot\sum_i^N \gamma\boldsymbol{I}_i$.

In the presence of both the static and the rf fields, the primary motion of each spin is the precession about an effective field $\boldsymbol{\Omega}_{\mathbf{e}}/\gamma = (B_1, 0, B_0 + \omega/\gamma)$, which itself rotates with frequency ω around the z axis; see Fig. 1. The effective frequency vector $\boldsymbol{\Omega}_{\mathbf{e}}$ of this doubly rotating frame has length $\Omega_{\mathrm{e}} = \mathrm{sgn}(\gamma)\sqrt{\Omega_1^2 + (\Omega_0+\omega)^2}$ and makes angle $\alpha = \mathrm{arccot}\frac{\Omega_0+\omega}{\Omega_1}$ with respect to the z axis. In this case, the Van Vleck–Redfield two-step truncation [25] of the Hamiltonian (1) gives the effective secular Hamiltonian [26]:

$$\mathcal{H}'_{\mathrm{sec}} = \left\langle\langle\mathcal{H}'_{\mathrm{DD}}\rangle_{B_0}\right\rangle_{B_1} = \frac{3\cos^2\alpha - 1}{2} \times \sum_{i<j} b_{ij}\left(1 - \frac{3r_{ij,z}^2}{r_{ij}^2}\right)\left(I_i'^z I_j'^z - \frac{1}{4}(I_j'^+ I_k'^- + I_j'^- I_k'^+)\right), \tag{2}$$

where the operators $\boldsymbol{I}'_i$ are defined in the doubly rotating reference frame $(x^{\omega,\alpha,\Omega_{\mathrm{e}}}, y^{\omega,\alpha,\Omega_{\mathrm{e}}}, z^{\omega,\alpha})$, see Fig. 1, that defines the axes for $I_k'^z$: $I_k'^{\pm} = I_k'^x \pm iI_k'^y$. The above Hamiltonian is called "secular," because the dynamics governed by it conserve the total spin projection $\sum_i I_i'^z$ onto the direction of $z^{\omega,\alpha}$. We illustrate the cancellation of oscillating nonsecular terms

$$\mathcal{H}'_{\mathrm{ns}} = \mathcal{H}'_{\mathrm{DD}} - \mathcal{H}'_{\mathrm{sec}} = \sum_{i<j}^{N} b_{ij}\boldsymbol{I}'_i\hat{\boldsymbol{A}}_{ij}^{\mathrm{ns}}(t)\boldsymbol{I}'_j \tag{3}$$

for a pair of spins irradiated on Larmor frequency and off resonance in Figs. 1(e) and 1(g), respectively. In both cases the two rotation frequencies ω and Ω_{e} are sufficiently incommensurate such that $x^{\omega,\alpha,\Omega_{\mathrm{e}}}$ and $y^{\omega,\alpha,\Omega_{\mathrm{e}}}$ axes as seen from the laboratory frame follow open paths that densely cover the $\pm\alpha$ zone around the equator as shown in Figs. 1(d) and 1(f).

The situation changes in the presence of NSRs, when the two rotation frequencies match certain commensurate ratios $\omega/\Omega_{\mathrm{e}} \in \{\pm 1/2, -1, -2\}$. Then the axes of the doubly rotating frame follow closed paths as shown for an example in Fig. 1(h). In analogy to perturbations for resonant tori in KAM theory [15–19], nonsecular terms still oscillate, but no longer average to zero over time as shown in Fig. 1(i).

In this work, we verify the effect of one of five predicted NSRs [7], referred to as NSR1 in the Supplemental Material (SM) [27]:

$$\omega = \frac{-4\Omega_0 - 2\sqrt{\Omega_0^2 - 3\Omega_1^2}}{3} \approx -2\Omega_0, \tag{4}$$

which gives the largest correction to the secular approximation under the condition $B_1 \ll B_0$ representative of our experiments [7,8]. In this case, the time-averaged nonsecular correction to the secular Hamiltonian (2) has the form

$$\langle\mathcal{H}'_{\mathrm{ns}}\rangle_{B_0,B_1} = \frac{3}{4}[\sin(2\alpha) - 2\sin(\alpha)] \times \sum_{i<j}^{N}\frac{\gamma_i\gamma_j\hbar^2}{r_{ij}^3}\left[\frac{r_{ij,x}r_{ij,z}}{r_{ij}^2}(I'_{ix}I'_{jx} - I'_{iy}I'_{jy}) - \frac{r_{ij,y}r_{ij,z}}{r_{ij}^2}(I'_{ix}I'_{jy} + I'_{iy}I'_{jx})\right]. \tag{5}$$

Unlike the secular term in Eq. (2), $\mathcal{H}_{\mathrm{ns}}$ does not conserve $\sum_i I_i'^z$. Hence all projections of the total spin polarization decay to zero under the combined action of $\mathcal{H}_{\mathrm{sec}}$ and $\mathcal{H}_{\mathrm{ns}}$. Under the conditions of our experiments corresponding to $B_1/B_0 \ll 1$, the projection $\sum_i I_i'^z$ should exhibit the slowest decay, which, however, can be much faster than the spin-lattice relaxation time T_1.

TABLE I. Nomenclature of frequencies in this manuscript.

Symbol	Description	Definition
ω	Frequency of applied rf field B_1	
Ω_0	Larmor frequency due to B_0	$\Omega_0 = \gamma B_0$
Ω_1	Nutation frequency due to B_1	$\Omega_1 = \gamma B_1$
Ω_{e}	Effective nutation frequency due to B_{e}	$\Omega_{\mathrm{e}} = \gamma B_{\mathrm{e}}$

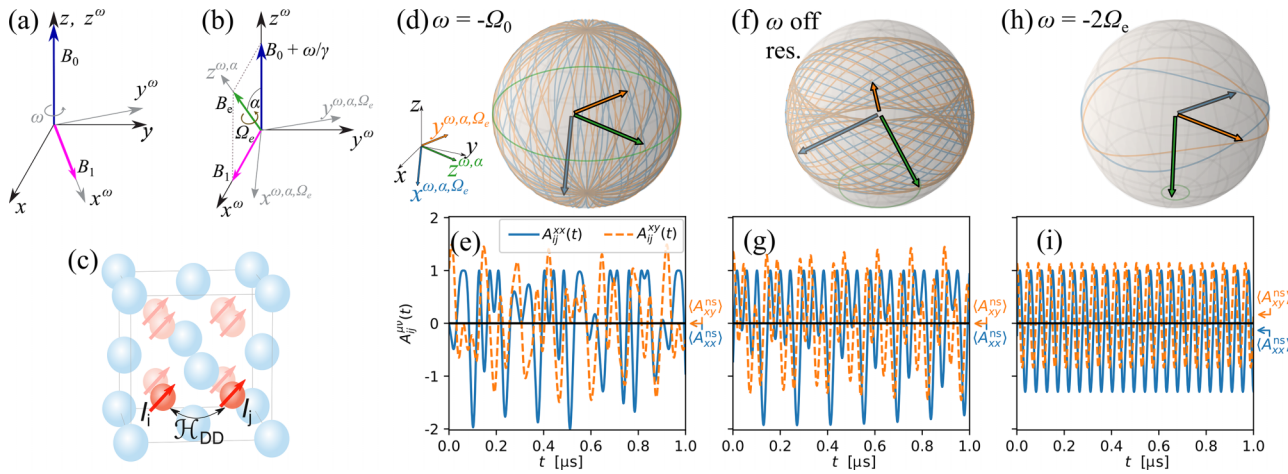

FIG. 1. NS interaction of two spins in the doubly rotating frame. (a) The rotating frame $(x^\omega, y^\omega, z^\omega)$ revolves about the laboratory frame's z axis with rf ω. (b) The rf field B_1 is static in the rotating frame, so the effective field $B_e = (B_1, 0, B_0 + \omega/\gamma)$, which is tilted by α from B_0. The doubly rotating frame $(x^{\omega,\alpha,\Omega_e}, y^{\omega,\alpha,\Omega_e}, z^{\omega,\alpha})$ precesses with $\Omega_e = \gamma B_e$ about B_e. Nuclear spins that interact only with B_0 and B_1 would be at rest in this doubly rotating frame, but are perturbed by the dipolar coupling, which, after the transformation to that frame, acquires a time-dependent interaction tensor $\hat{\boldsymbol{A}}_{ij}(t)$—see Eq. (3). (c) Two dipolar-coupled ^{19}F spins i and j in the CaF_2 crystal lattice. Panels (d), (f), and (h) each represent the motion of the unit vectors (blue, orange, and green) of the three axes of the double-rotating frame when viewed in the laboratory frame, under different resonance conditions. Panel (d) represents a Rabi rotation under resonant condition $\omega = -\Omega_0$ in a typical NMR experiment: the tips of the unit vectors evolve along open trajectories covering the entire unit sphere. (e) Then nonsecular terms in the dipolar interaction matrix, such as $A_{ij}^{xy}(t)$ and $A_{ij}^{xx}(t)$, oscillate irregularly and average over time to zero (marked by arrows on the right abscissa indicate). (f) If the frequency of $B_1(t)$ is off resonance (here about $-1.3\Omega_0$) the unit vectors likewise follow open trajectories, albeit covering the unit sphere only partially, and (g) oscillating nonsecular terms again average to zero. (h) If however the rf is set to match a NSR condition, the unit vectors of the doubly rotating frame evolve along closed trajectories and (i) the nonsecular terms oscillate regularly and can exhibit nonzero averages. The displayed numerical averages of Eq. (3) over 1 μs match the prediction of Eq. (5), i.e., $\langle A_{ij}^{xx} \rangle = -\langle A_{ij}^{xy} \rangle = 0.15 = \frac{3}{4}[\sin(2\alpha) - 2\sin(\alpha)] \cdot r_{ij,x} r_{ij,z}/r_{ij}^2$, for the simulated two nearest-neighbor ^{19}F spins with B_0 along the (111) direction, $\Omega_0/2\pi = 11$ MHz and $\Omega_1/\Omega_0 = 0.15$.

The time constant T_{ns} associated with the nonsecular decay of $\sum_i I_i^z$ can be estimated [8] as

$$T_{ns} = \frac{b_{loc}^{sec}}{\gamma \left(b_{loc}^{ns}\right)^2}. \tag{6}$$

Here b_{loc}^{sec} and b_{loc}^{ns} refer to the root mean squares of the local secular and nonsecular dipolar fields, respectively, seen by each nuclear spin. The calculation of the local fields is detailed in the SM.

Fast-field-cycling experiments. We investigate NSRs with just one rf frequency $\omega = 2\pi \times 21.7$ MHz. Using fast changes of B_0, we can first irradiate at a field ($B_0 \approx 1/2B_{res}$), where ω fulfills the NSR condition (4), $\omega \approx -2B_0 \cdot \gamma$, and then goes to resonance field ($B_0 = B_{res}$), where $\omega = -B_0 \cdot \gamma$ matches the Larmor frequency to read out the effect on the nuclear magnetization.

The measurements were performed using a fast-field-cycling (FFC) setup [28,29], previously located at Nottingham University and now in use at the Karlsruhe Institute of Technology with updated interfaces. The system has a temperature range from 3 to 300 K and magnetic field range from 0 to about 2.5 T, with an absolute error of 2 mT. All experiments described here were performed at 200 K and the field ramps performed at a rate of 2.8 T/s. A Bruker spectrometer was used for NMR measurements as well as control of the FFC magnet from within the NMR pulse sequence; for details see the SM. Our home-built NMR probe is equipped with a solenoid tuned to frequency of 21.7 MHz, which, for ^{19}F, corresponds to a resonant magnetic field B_{res} of 0.544 T.

The sample is a single crystal of CaF_2 (MaTeK, Germany) cut into cylindrical shape ($d = 5$ mm, $l = 1$ cm) with a (110) axis along the cylinder axis, such that all axes of interest can be aligned with the external field B_0. For further experimental details, see the SM.

The principle FFC experiment is depicted in Fig. 2 and consists of three stages: (I) a *preparation* stage, where a well-defined spin polarization is established, followed by (II) an *evolution* stage where the spins evolve for the time t_{evo} at the field of interest B_{evo}, and (III) the *readout* of the resulting polarization. In order to detect NSR effects, we fulfill Eq. (4) by setting B_{evo} to half of B_{res}, such that the (unchanged) rf frequency ω is now twice the Larmor frequency, and irradiate during stage II.

We probe the NSR in two versions of the FFC experiment shown in Fig. 2. In *NSR sweeps* we irradiate at different evolution fields varied around $B_{evo} = B_{res}/2$. This tests the NSR condition Eq. (4) and the diminished signal indicates a NSR. In *NSR decay measurements* we drive the NSR (at different rf powers) for a varying t_{evo} and determine $T_{ns}(B_1)$ by measuring $M_z(t_{evo})$. This experiment probes the quantitative prediction Eq. (6).

Owing to the limited precision of the FFC magnet $\Delta B_{FFC} = 2$ mT all experiments were repeated several times.

In both types of experiments there are two contributions to the total relaxation. If the NSR is not driven (corresponding to

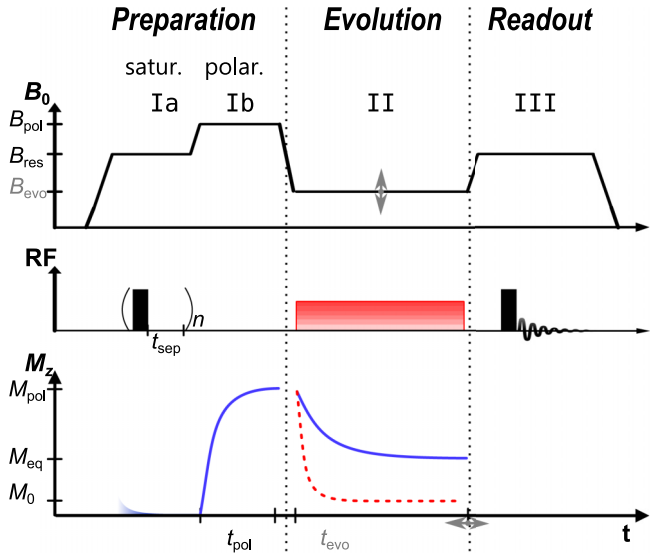

FIG. 2. Scheme of FFC NMR experiments in terms of applied static field B_0 (top panel), applied rf pulses (center panel), and corresponding nuclear spin magnetization (bottom panel). In the *Preparation* stage the field is initially ramped to resonance field B_{res} ($B_{res} \cdot \gamma = \omega = 2\pi \times 21.7$ MHz) and any nuclear polarization is saturated in step Ia by a train of $n \sim 10^2$–10^3 pulses separated by $t_{sep} = 1$ ms. A well defined polarization is built up in step Ib over a time t_{pol} at field B_{pol}. For experiments reported herein, $t_{pol} = 100$ s at $B_{pol} = B_{res}$. In the *Evolution* stage (II) the spin system is allowed to relax at a B_{evo} for a variable time t_{evo}. This is followed by (III) a ramp back to B_{res} for the magnetization *Readout*. For NSR detection we additionally apply rf (ω) irradition (red box) of variable power (0–30 W) during the evolution stage (II). If the NSR condition is matched ($\Omega_0 = \gamma B_{evo} = \frac{1}{2}\omega$), faster relaxation to a lower stationary magnetization (dashed red line) is expected. Otherwise the regular spin-lattice relaxation to equilibrium magnetization will be observed (full blue line).

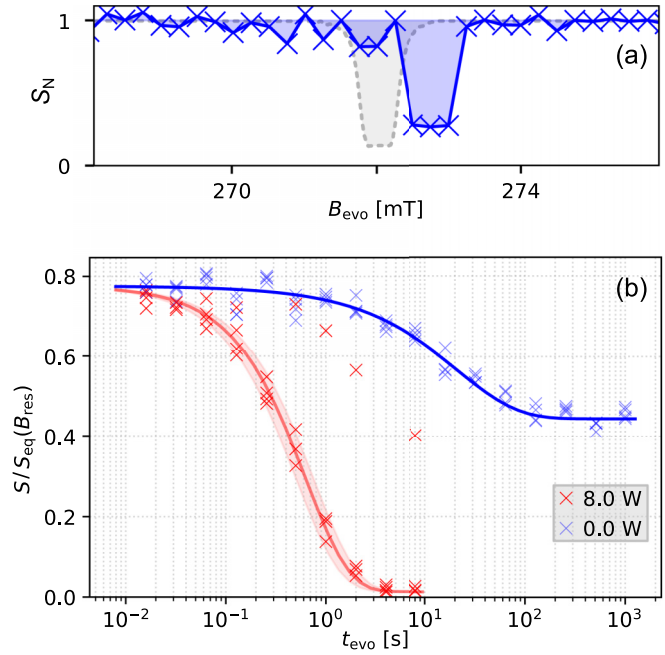

FIG. 3. (a) *NSR sweep* example for the (111) orientation of B_0, obtained by measuring polarization decay for different B_{evo} and rf irradiation (30 W) for $t_{evo} = 2$ s. Signals normalized to nondissipative relaxation. Also indicated is the expected NSR (*gray*) at $B_{evo} = B_{res}/2 = 272$ mT with width corresponding to dipolar (secular) dominated ^{19}F NMR linewidth (24 kHz) for this crystal orientation in CaF_2 and the limited precision of the FFC setup $\Delta B_{FFC} = 2$ mT; see text. (b) *Nonsecular vs spin-lattice relaxation:* polarization decay experiments at $B_{evo} = \frac{1}{2}B_{res}$ for varying t_{evo}. The signal intensity S is normalized to equilibrium signal at $B_{res} = 0.544$ T. Without irradiation (blue) the signal decays slowly [$T_1(0.27\ \text{T}) = 21$ s] to the equilibrium value for $1/2B_{res}$ [$S/S_{eq}(B_{res}) = 0.5$]. With irradiation (red) the signal decays much faster to a smaller steady state value. We repeated each experiment five times since field drifts and offsets can frustrate NSR conditions, leading to some data points closer to regular spin-lattice relaxation. Disregarding outliers we find $T_{ns} = 0.65 \pm 0.13$ s.

off-resonant irradiation in NSR sweeps or zero power in NSR decay measurements), the magnetization (M_{pol}) will decay to the equilibrium value $M_{eq}(B_{evo})$ at B_{evo} with its spin-lattice relaxation time constant, $\dot{M}_z = -(M_z - M_{eq})/T_1$. Due to the short ramp times ($\ll T_1$) we ignore relaxation effects during ramps. In stage III the signal is then proportional to

$$M_z(t_{evo}) = M_{eq} + (M_{pol} - M_{eq}) \cdot e^{-t_{evo}/T_1} \tag{7}$$

as indicated (full blue line) in the bottom panel of Fig. 2.

Upon driving the NSR, the predicted relaxation term $-M_z/T_{ns}$ adds to the rate of change of the magnetization $\dot{M}_z$. The resultant relaxation [8] is then toward a lower steady-state magnetization $M_0 = M_{eq}(T_{ns})/(T_{ns} + T_1)$ with a faster relaxation rate $T_0^{-1} = T_{ns}^{-1} + T_1^{-1}$:

$$M_z(t_{evo}) = M_0 + (M_{pol} - M_0) \cdot e^{-t_{evo}/T_0}, \tag{8}$$

as indicated (red dashed line) in the bottom panel of Fig. 2.

NSR sweeps provide a qualitative probe of the NSR condition. For rf irradiation fulfilling the NSR condition $B_{evo} = B_{res}/2 = 272$ mT we expect a suppression of the signal, whereas irradiation off NSR should not affect the signal. Figure 3(a) shows an example of such a sweep (×) that matches the expected suppression (indicated in gray), except for a shift by about +0.5 mT. The width of the NSR, i.e., the signal suppression, corresponds to the dipolar NMR linewidth given by the secular part of the dipolar field Eq. (2), as expected. In all sweeps in each direction we find a NSR effect qualitatively matching the expectation, i.e., a diminished signal near the NSR condition with a width on the order of the dipolar line shape. Repeated sweeps under the same conditions, however, yield varying results which we attribute to the uncertainty in the B_0 field (±2 mT); for more examples see the SM.

NSR decay measurements test the quantitative prediction. We drive the NSR $B_{evo} = 1/2B_{res}$, determine T_{ns} from $M_z(t_{evo})$ as a function of rf power according to Eq. (8), and compare the result to Eq. (6). Note that both parameters, the time constant T_0 as well as the final polarization M_0, provide measures of T_{ns}. To compensate for the uncertainty in B_0 in matching the NSR condition, we vary the rf frequency ω during irradiation by ±40 kHz ($\widehat{=}$ ±1 mT) thereby covering a bandwidth of $\Delta_{rf} = 80$ kHz [30] in the NSR decay measurements and repeat all measurements several times.

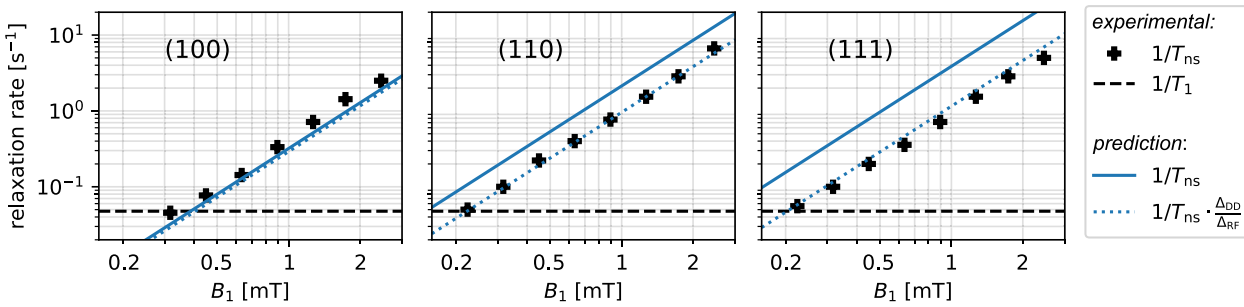

FIG. 4. NSR dissipation rates T_{ns}^{-1} measured (symbols) in the three directions as functions of B_1 and compared to the theoretical predictions (6) for the investigated NSR (full lines). Dotted lines are the same theoretical predictions corrected by a prefactor accounting for the effective irradiation time; see text.

In Fig. 3(b) we show the results for the (111) orientation without and with irradiation of 8 W rf power. Each experiment was repeated five times leading to multiple points for each t_{evo}. In either case, with and without irradiation, we start for small t_{evo} with the previously built-up polarization (of about 80% of equilibrium magnetization at B_{res}; see the SM for details).

Without irradiation (0 W, blue) the polarization decays via regular spin-lattice relaxation to the equilibrium value, which at $\frac{1}{2}B_{res}$ is half of that at B_{res}.

With irradiation (8 W, red) we find that most data points reflect a much faster relaxation to a much lower steady-state polarization, as predicted for NSR irradiation. Some outliers closer to the 0 W curve reflect experiments where spontaneous field offsets lead to a mismatch for the NSR condition.

We have performed such polarization decay experiments with NSR irradiation of varying rf power (0–30 W) similarly multiple times for all three orientations, (111), (110), and (100); see the SM. The experimentally determined T_{ns}^{-1} are shown in Fig. 4 as a function of the applied B_1 field strength as determined from nutation experiments; see the SM for details. The measured NSR dissipation rates (symbols) exceed the spin-lattice relaxation rate (dashed lines) in all orientations already for low values of B_1 and show the expected quadratic dependence. Also shown are the theoretical predictions for T_{ns}^{-1} (full blue lines). For the (100) direction the data match the prediction fairly well. While the measured NSR dissipation is faster in (110) and (111), as expected, the measured rates are below the predictions. Here, we have to take into account the range of the rf frequency sweep during NSR irradiation, $\Delta_{rf} = 80$ kHz in relation to the dipolar linewidth, which differs for the three directions, with $\Delta_{DD} = 73,\ 36,$ and 24 kHz for the (100), (110), and (111) directions, respectively; for details see the SM.

Scaling the predicted rates by the factor Δ_{DD}/Δ_{rf}, corresponding to the effective time during which the resonance is driven (dotted lines), gives a good match between prediction and observed relaxation rates.

Conclusion. We have reported an observation of a nonsecular resonance, a magnetic resonance of a dipolar coupled spin 1/2 system at a fractional multiple of the Larmor frequency. The results provide qualitative proof of the effect's resonant nature and are in quantitative agreement with the predicted relaxation rates. While in this work CaF_2 serves as a test bed with exactly defined dipolar couplings, the existence of NSRs is anticipated for any sample with dipolar coupled spins. The observation is made possible through the adaptation of a fast-field-cycling apparatus that enables excitation and detection at different fields. Thereby large ratios of the radio-frequency and static fields can be achieved while working with the equilibrium polarization of a higher field. We note that the NSR reported here could also be observed at a static field using a double-resonant probe, provided that a sufficiently high $B_1/B_0 \gtrsim 1\%$ can be achieved. The reported effects are dissipative in nature and provide a mechanism to saturate dipolar coupled spins. Specifically it should be possible to saturate spins at frequencies as low as 1/3 of the Larmor frequency. Experiments to probe other homonuclear NSRs below the Larmor frequency are in preparation.

We furthermore work on experiments to probe heteronuclear NSRs that can drive cross polarization between two nuclear spin species.

Acknowledgments. We thank J. R. Owers-Bradley, J. F. MacDonald, and A. J. Horsewill for donating their field-cycling apparatus to our laboratory. B.V.F. thanks B. Eaton and G. Eaton for a discussion. This work has been supported by the "Impuls- und Vernetzungsfonds of the Helmholtz-Association" under Grant No. VH-NG-1432 and received funding from the European Research Council (ERC) under the European Union's Horizon 2020 research and innovation program (Grant Agreement No. 951459). B.M. acknowledges support from the Deutsche Forschungsgemeinschaft (DFG, Grant No. 454252928, SFB 1527).

Data availability. The data that support the findings of this Letter are openly available [27], embargo periods may apply.

[1] S. R. Hartmann and E. L. Hahn, Nuclear double resonance in the rotating frame, Phys. Rev. **128**, 2042 (1962).

[2] A. Henstra, P. Dirksen, J. Schmidt, and W. Wenckebach, Nuclear spin orientation via electron spin locking (NOVEL), J. Magn. Reson. **77**, 389 (1988).

[3] M. Bloom and M. A. LeGros, Direct detection of two-quantum coherence, Can. J. Phys. **64**, 1522 (1986).

[4] I. M. Haies, J. A. Jarvis, H. Bentley, I. Heinmaa, I. Kuprov, P. T. F. Williamson, and M. Carravetta, ^{14}N overtone NMR under MAS: Signal enhancement using symmetry-based

sequences and novel simulation strategies, Phys. Chem. Chem. Phys. **17**, 6577 (2015).

[5] Y. Zur, M. H. Levitt, and S. Vega, Multiphoton NMR spectroscopy on a spin system with $I = 1/2$, J. Chem. Phys. **78**, 5293 (1983).

[6] S. S. Eaton, K. M. More, B. M. Sawant, and G. R. Eaton, Use of the ESR half-field transition to determine the interspin distance and the orientation of the interspin vector in systems with two unpaired electrons, J. Am. Chem. Soc. **105**, 6560 (1983).

[7] C. M. Kropf and B. V. Fine, Nonsecular resonances for the coupling between nuclear spins in solids, Phys. Rev. B **86**, 094401 (2012).

[8] C. M. Kropf, J. Kohlrautz, J. Haase, and B. V. Fine, Anomalous longitudinal relaxation of nuclear spins in CaF_2, Fortschr. Phys. **65**, 1600023 (2017).

[9] J. H. V. Vleck, The dipolar broadening of magnetic resonance lines in crystals, Phys. Rev. **74**, 1168 (1948).

[10] A. G. Redfield, Nuclear magnetic resonance saturation and rotary saturation in solids, Phys. Rev. **98**, 1787 (1955).

[11] C. P. Slichter, *Principles of Magnetic Resonance* (Springer, Berlin, 1990).

[12] M. H. Levitt, *Spin Dynamics: Basics of Nuclear Magnetic Resonance* (John Wiley & Sons, Ltd., New York, 2008).

[13] R. R. Ernst, G. Bodenhausen, and A. Wokaun, *Principles of Nuclear Magnetic Resonance in One and Two Dimensions* (Oxford University Press, Oxford, UK, 1987).

[14] A. Abragam and M. Goldman, *Nuclear Magnetism: Order and Disorder* (Oxford University Press, Oxford, UK, 1982).

[15] A. N. Kolmogorov, On the conservation of quasiperiodic motions for a small change in the Hamiltonian function, Dokl. Acad. Nauk USSR **98**, 527 (1954).

[16] J. Moser, On invariant curves of area-preserving mappings of an annulus, Nach. Akad. Wiss. Göttingen, Math. Phys. Kl. II **1**, 1 (1962).

[17] V. I. Arnol'd, Small denominators and problems of stability of motion in classical and celestial mechanics, Russ. Math. Surv. **18**, 85 (1963).

[18] B. V. Chirikov, A universal instability of many-dimensional oscillator systems, Phys. Rep. **52**, 263 (1979).

[19] V. I. Arnold, *Mathematical Methods of Classical Mechanics* (Springer, New York, 1978).

[20] In keeping with Ref. [7], we use the definition $\Omega_0 = +\gamma B_0$, opposite in sign to the more common definition. Owing to this, e.g., irradiation on resonance for Rabi rotation is at $\omega = -\Omega_0$ as shown in Fig. 1(d).

[21] The signs of the nonsecular resonances are immaterial for our experiments, since the applied rf field is linearly polarized. The field is written as a superposition of two counter-rotating circularly polarized fields, and only the circularly polarized part with the correct sign/polarization affects the spins.

[22] S. W. Morgan, B. V. Fine, and B. Saam, Universal long-time behavior of nuclear spin decays in a solid, Phys. Rev. Lett. **101**, 067601 (2008).

[23] B. Meier, J. Kohlrautz, and J. Haase, Eigenmodes in the long-time behavior of a coupled spin system measured with nuclear magnetic resonance, Phys. Rev. Lett. **108**, 177602 (2012).

[24] H. Cho, T. D. Ladd, J. Baugh, D. G. Cory, and C. Ramanathan, Multispin dynamics of the solid-state NMR free induction decay, Phys. Rev. B **72**, 054427 (2005).

[25] To emphasize averaged Hamiltonians, we use $\langle\langle \ldots \rangle_{B_0} \rangle_{B_1}$ to denote the consecutive averages over the action of B_0 and B_1 in the Van Vleck–Redfield two-step truncation. The averaging over the full rotation after Kropf and Fine [7] is denoted by $\langle \ldots \rangle_{B_0,B_1}$.

[26] In this work we explicitly mark doubly rotating frame Hamiltonians using the $'$ symbol. In the earlier works [7,8], the frame is defined implicitly via the spin operators that appear within the Hamiltonian.

[27] See Supplemental Material at http://link.aps.org/supplemental/10.1103/h2sn-wvzm for details regarding the predictions for all five homonuclear NSRs as well as additional experimental details and supplementary data.

[28] A. J. Horsewill and Q. Xue, Magnetic field-cycling investigations of molecular tunnelling, Phys. Chem. Chem. Phys. **4**, 5475 (2002).

[29] D. T. Peat, M. L. Hirsch, D. G. Gadian, A. J. Horsewill, J. R. Owers-Bradley, and J. G. Kempf, Low-field thermal mixing in [1-^{13}C] pyruvic acid for brute-force hyperpolarization, Phys. Chem. Chem. Phys. **18**, 19173 (2016).

[30] We increased the frequency by 5 kHz every 1 ms (990 μs irradiation with 10 μs breaks).